Influence of crosslinking density of a cataphoretic coating on initiation and propagation of filiform corrosion of AA6016

A.-P. Romano [a,*], M.-G. Olivier [a], A. Nazarov [b], D. Thierry [b]

[a] Service de Science des Matériaux, Faculté Polytechnique de Mons, Mons, Belgium
[b] French Corrosion Institute, Technopole de Brest Iroise-220, rue Pierre Rivoalon, 29200 Brest, France

ARTICLE INFO

ABSTRACT

The effect of curing temperature on initiation and propagation of filiform corrosion of an epoxy cataphoretic electrocoating deposited on aluminum alloy substrate was studied. EIS measurements were used to follow the evolution of the water uptake of the intact coatings. In addition, EIS was applied to determine the performances of the systems as a result of exposure to HCl vapours.

Cantilever method (stressmeter) was used to determine the stresses generated in an organic coating during a humidity cycle.

Scanning Kelvin Probe (SKP) was applied in order to investigate the initiation and propagation of filiform corrosion of painted aluminum alloy. The mechanism of filiform corrosion is discussed according to the paint properties.

© 2009 Published by Elsevier B.V.

1. Introduction

A large amount of metallic constructions in atmospheric weathering conditions are protected by polymeric (paint) coatings. Different studies have been carried out in order to determine the mechanisms of corrosion beneath the coating. The development of filiform corrosion underneath organic coatings on steel, aluminum and magnesium alloys, results in thread-like corrosion products which propagate across the coating–metal interface. All details were reviewed in [1–3]. Filiform corrosion is most virulent in an environment with a combined marine (presence of anion chloride) and industrial atmosphere [2]. It can be controlled by many parameters such as metallic substrate surface pretreatment, defects, permeability of the coating to water and oxygen, adherence of the paint system and salts. The adhesion and stability of the metal–coating interface are controlling the initial stage of degradation [4].

The filament can be divided in two parts, namely a head where active metal dissolution takes place and a tail composed of corrosion products. Most explanations are based on the differential oxygen concentration cell mechanism, as suggested in [5]. The oxygen concentration is high in the tail, where it is reduced and is low in the active head, where metal anodic oxidation takes place.

It is generally accepted that the mechanism of filiform corrosion is the anodic undercutting of the coating by the filament. Visualizing the galvanic cell "*in situ*" underneath polymeric coatings was made possible thanks to Scanning Kelvin Probe (SKP) or Atomic Force Microscopy in Kelvin Probe Mode [6–9].

SKP is a useful method to investigate filiform corrosion because it does not require bulk electrolyte and it can measure the potential below thin adsorbed electrolyte films or resistive intact polymeric coatings. In this study, SKP was applied to study filiform corrosion of aluminum alloy AA6016 coated with cataphoretic epoxy coating. This alloy painted and cured at 185 °C had previously been studied by FT-IR and SKP in [7]. The electrocoating was also characterized previously [10] and the influence of curing temperature (155, 165, 175, 185 and 195 °C) on the mechanical properties was proved.

The filiform corrosion resistance of coated Al6016 substrates was determined by a normalized test (ISO/DIS 4623) and by electrochemical impedance spectroscopy on scratched samples. After optimizing the experimental parameters, the active area of various systems vs. immersion times in electrolyte solution was determined by EIS [10]. It was shown that by increasing the temperature, the density of the crosslinking bonds in the polymer matrix also increases. The lowest active area was obtained at 175 °C. For curing temperatures lower than 175 °C, a disbonding phenomenon was observed. A good correlation was observed between the results obtained by the normalized test (21 days) and by EIS within a shorter time (24 h).

The aim of this work was to continue these investigations and, in particular, to study, through different techniques, the influ-

* Corresponding author.
 E-mail address: anne-pascale.romano@fpms.ac.be (A.-P. Romano).

Table 1
Chemical composition (weight%) of aluminum alloy AA6016.

	Weight%
Al	97.900
Si	1.184
Mg	0.318
Fe	0.300
Mn	0.126
Cu	0.118
Balance	0.054

ence of the curing conditions of a cataphoretic coating on its mechanical properties and its filiform corrosion performances on AA6016 aluminum alloy. The parameters investigated are wet adhesion, water uptake, stress generated in the organic coatings and their evolution behaviour with regard to temperature and humidity. The techniques used were EIS and the cantilever method [11–14]. Presently the stress measurements can only be carried out on a calibrated steel substrate. This explains why steel was used in some experiments for paint characterization. The study of the influence of test conditions and mechanisms of initiation and development of filiform corrosion was carried out on intact samples by EIS measurements and on scratched samples by SKP measurements.

2. Experimentation

2.1. Materials and exposure

For stress measurements, electrocoating was applied on a calibrated substrate made of carbon steel (282 mm × 12.6 mm × 0.1 mm) degreased with acetone. In order to obtain a thickness of 15 μm, the applied voltage was 100 V and the bath temperature 30 °C. The samples were coated for 2 min 30 s, rinsed and cured for 25 min.

The panels of aluminum alloy AA6016 (the composition of this alloy is summarized in Table 1) were degreased, etched for 10 min in a commercial bath (Ridoline® 124N and Novox Activator 12B by Henkel S.A.) and subsequently rinsed with deionised water before coating. The applied voltage was determined in order to obtain a film thickness of 20 μm. The bath temperature was 30 °C. The samples were coated for 3 min, rinsed and cured in an oven for 25 min.

The curing temperatures were 155, 165, 175, 185 and 195 °C. After curing, the film thicknesses were measured with a 456 Elcometer thickness gauge.

For testing painted aluminum samples by SKP measurement scratches of 1 mm wide were made. According ISO/DIS 4623 the samples were exposed during 1 h in HCl vapours to initiate filiform corrosion. The samples were then exposed in a climatic chamber at 40 °C and 80% RH during 21 days.

2.2. Stress measurements

2.2.1. Stress interpretation

There is now no doubt that stress can affect coating adhesion and that this may lead to delamination or filiform corrosion. As seen in [15], stress leads to peeling out and lifting of the coating under conditions of cathodic delamination that facilitates degradation. This parameter should also influence the propagation of filiform corrosion.

The three main causes of stress development in an organic coating are: film formation, variations in temperature and in relative humidity (RH) [11–14]. The kinds of stress arising are known as internal (S^F), thermal (S^T), and hygroscopic (S^H), respectively. The

thermal and hygroscopic stresses are often referred to as hydrothermal stresses. The total stress is defined as follows:

$$S_{tot} = S^F \pm S^T \pm S^H \tag{1}$$

For coatings that can contract or expand only through their thickness, Eq. (2) represents the simplified general equation describing the stress arising in a coating:

$$S = \frac{E\varepsilon}{1 - \upsilon}. \tag{2}$$

One can also write that

$$S^F = \int_{V_S}^{V_t} \frac{E}{1 - \upsilon} \frac{1}{3V_S} dV. \tag{3}$$

where S is the stress (N/m²), ε the strain, υ the Poisson's ratio, E the elastic modulus (N/m²), and V_S and V_t are the volumes of the coating at solidification and at time t after solidification, respectively.

When coated substrates are exposed to variations in temperature and humidity, dimensional changes are induced. If the thermal and hygroscopic expansion coefficients of the coating (α_F^T and α_F^H) and the substrate (α_S^T and α_S^T) are different, which is usually the case, thermal and hygroscopic stresses (S^T and S^H) will develop in the coating.

$$S^T = \int_{T_1}^{T_2} \frac{E}{1 - \upsilon} (\alpha_F^T - \alpha_S^T) \, dT \tag{4}$$

$$S^H = \int_{RH_1}^{RH_2} \frac{E}{1 - \upsilon} (\alpha_F^H - \alpha_S^H) \, dRH \tag{5}$$

In practice, these stresses act together. The positive sign denotes a coating tendency to contract (tensile stress) and the negative sign a coating tendency to expand (compressive stress). S^F is practically always positive.

Two climatic conditions can lead to high stress in a coating:

1. Low temperatures and RH's induce high tensile stresses;
2. High temperatures and RH's induce high compressive stresses.

2.2.2. Method

The method used to measure stress is based on the cantilever method (based on Perera and Schutyser's research work [11]). This method is based on the following: if a coating under stress is applied on a substrate, the coated substrate will deflect in the direction which relieves stress. Since deflection can be measured and the elastic properties of the substrate are known from separate determinations, stress can be calculated.

The mathematical equation to calculate stress is the following:

$$S = \frac{4d' E_s t^3}{3l^2 c(t+c)(1 - \upsilon_s)} + \frac{4d' E_c(t+c)}{l^2(1 - \upsilon_c)} \tag{6}$$

where d' is the deflection in the middle of the substrate (m), E_s the elastic modulus of the substrate (N/m²), E_c the elastic modulus of the coating (N/m²), υ_s the Poisson's ratio of the substrate, υ_c the Poisson's ratio of the coating, t the thickness of the substrate (m), c the thickness of the coating (m), and l is the distance between the two knife edges (m).

Eq. (6) assumes a good adhesion between the coating and the substrate, and isotropic elastic properties of the coating and the substrate. It also assumes that the elastic limit of the substrate is not exceeded and that the stress is constant throughout the coating thickness.

The second term in Eq. (6), which contains a number of coating properties difficult to determine, can be neglected, as, in that case, $E_s \gg E_c$ and $t \gg c$.

A commercial equipment, the CoRi stressmeter was used to measure the deflection in the middle of the substrate. The stress evolution of an uncoated substrate, used as reference, is always subtracted from data obtained with a coated one. For each condition, measurements were repeated three times.

2.3. Electrochemical measurements

2.3.1. EIS method and equipment

EIS measurements were carried out on intact samples with a conventional three-electrode cell in order to determine water uptake of electrocoatings and the stability of adhesion in water electrolyte. The working electrode was the investigated sample (exposed area of $4.5\,cm^2$), the counter electrode was a platinum plate and all potentials were measured with respect to an Ag/AgCl reference electrode. The cell was filled with a NaCl 0.5 M solution and placed in a Faraday cage in order to minimize external interference on the system. The impedance measurements were carried out over frequencies ranging from 100 kHz to 10 mHz using a 20 mV rms amplitude signal voltage, at ambient temperature. The impedance spectra were acquired by using a frequency response analyser and potentiostat, both devices being computer-controlled with Powersuite® software.

2.3.2. Interpretation of EIS data

The coating properties (adhesion and porosity) were characterized after different immersion times by following, on one hand, the changes of impedance modulus at low frequency (10 mHz) and, on the other hand, the coating capacitance determined from impedance values obtained at high frequencies [16,17].

The impedance values at the lowest frequency represent the total resistance of the system including pore resistance, resistance of electrochemical processes occurring at the exposed metal/electrolyte interface. Degradation of the metal–polymer joint can decrease the low frequency modulus. This is mainly due to the decrease in the pore resistance (e.g. due to polymer swelling) and the decrease in the interfacial resistance caused by corrosion reactions, loss of adhesion (e.g. blistering), when two time constants are visible in the impedance spectra.

The volume fraction of the water absorbed by the coating can be estimated from the capacitance data (C_c) by using the empirical formula derived by Brasher and Kingsbury [18]:

$$X_v = \frac{\log(C_c/C_0)}{\log 80} \tag{7}$$

where X_v is the volume fraction of water absorbed by the coating, C_0 the coating capacitance at the beginning of exposure (initial dry film capacitance) and 80 is the dielectric constant of water at room temperature.

2.3.3. Scanning Kelvin Probe (SKP)

The mechanical vibration of the probe above the working electrode creates an alternative capacitor ($C_{p/s}$) and an alternative current ($I(t)$) flowing between the probe and the working electrode surface. The amplitude of the current is related to a contact potential difference $\Delta V_{p/s}$ between the probe and the working electrode surfaces according to the following Eq. (8):

$$I(t) = \Delta V_{p/s} \frac{dC_{p/s}}{dt} \tag{8}$$

This potential drop corresponds to the difference in Volta potentials between the probe and the working electrode and is proportional to the difference in the electron work functions (Φ) (Eq.

(9)) [19].

$$\Delta V_{p/s} = \frac{\Phi_S - \Phi_P)}{e} \tag{9}$$

In this equation, e is the electron charge. The potential of the probe (Φ_P/e) is kept constant and calibrated against a reversible reference electrode. The potential (Φ_S/e) or work function (Φ_S) can thereby be obtained. Φ is defined as the minimal work to move the electron from the bulk of the metal to the point just outside its surface. The work function is thus the negative value of the real potential of an electron in a metal [20]. SKP can therefore be used to determine the corrosion or red-ox potentials of the metal surfaces in atmospheric environments [21].

According to the definition of the metal electron work function, Φ_S contains both bulk metal and surface contributions as seen in Eq. (10):

$$\frac{\Phi_S}{e} = \frac{\Phi_M}{e} + \phi_{m/o} + \phi_{o/a} \tag{10}$$

The electron in the bulk metal is determined by the Fermi energy (Φ_M) or chemical potential of an electron in the metal. For metals covered by oxide films, the metal is in contact with a semi-conductive oxide which creates a contact potential difference (Schottky junction $\phi_{m/o}$) which is equal to the difference in the work functions or Fermi levels before the materials came into contact [22]. SKP measures the potential in the air just outside the metal surface and the potential drop across oxide–air ($\phi_{o/a}$) contributes to the measured potential. Increasing the oxide film thickness proportionally raises the contact potential difference. This potential drop can help to determine the oxide film thickness on the aluminum alloys [23,24]. In SKP measurements the freshly polished Al has a potential close to $-0.6\,V$ (SHE) and its oxidation in the air enables the potential to reach $-0.3\,V$ (SHE) [25]. The SKP potential measured above a corroding location depends on the atmosphere. If humid air is replaced by humid nitrogen, the metal anodic polarization by oxygen red-ox system is inhibited and the corrosion potential drops by about 300 mV [25].

For metals covered by a polymer the potential measurements take place in the air above the surface of the organic coating. The oxide–air interface is replaced by metal oxide–polymer and polymer–air. According to the nature of the polymer and substrate, the adhesion bonding includes ionic, donor–acceptor or van der Waals interactions. These interactions can lead to charge separations at the interface. Hence, the polymer depending on its functional groups can raise or reduce the metal potential between 0.1 and 0.3 V [26]. On the other hand, the properties of the metal oxide underneath the coating can also affect the SKP potential measured above the intact metal–polymer interface [9]. As a consequence, the mechanical deformation of AA6016 surface decreases and the measured potential increases due to heat treatment [9].

The Volta potentials were measured by using a commercial Scanning Kelvin Probe from "UBM Messtechnik". The equipment can be used to measure the change in potential with time at a single point above the surface or to map the Volta potential over an area of the sample. SKP is equipped with an environmental chamber that makes it possible to carry out measurements in different atmospheres and humidities. The reference electrode was made of a Ni–Cr alloy with a tip diameter of about 80 μm. The distance between the needle and the sample was kept constant at 50 μm during measurement. This gives a lateral resolution ranging from 80 to 100 μm. The probe was calibrated in humid air (95% RH) above a Cu/CuSO4 saturated electrode and potentials were given with respect to a standard hydrogen electrode (SHE). The density of the measured points was 10 points/mm in X direction and 4 points/mm in Y direction.

Table 2
Glass transition values for different curing temperatures with a slope of thermal cycle of 60 °C/h [27].

Curing temperature (°C)	T_g (°C)
195	88.7
185	80.9
175	81.2
165	80.2
155	75.2

3. Results and discussion

3.1. Physical properties of the coatings

The stress measurements with respect to temperature were used to determine the glass transition temperatures. It is important to note that this T_g corresponds to the investigated metal–polymer interface and not only to the polymer phase. This temperature is related to the transfer from a vitreous state to a rubber state for the polymer linked to the metal. In this transition stage the internal residual stress built in at the interface relieves and T_g can be determined from stress measurement [10,27].

The painted samples were placed in the stressmeter and submitted to the following thermal cycle: from 40 to 130 °C with a slope of 60 °C/h at 15% RH. Table 2 gives the glass transition values for the coatings cured at different temperatures. These values were determined by using a thermal cycle of 60 °C/h.

At 185, 175, and 165 °C, the values of the glass transition are very similar. The lowest T_g value is obtained for samples cured at 155 °C and the higher T_g value for samples cured at 195 °C. The T_g values show that the crosslinking density increases when increasing the curing temperature.

3.2. Influence of the curing temperature on the water uptake measured by EIS

Fig. 1 shows the evolution of the water uptake, X_v, over 24 h, during immersion in a 0.5 M NaCl solution, at different curing temperatures. For all systems, the X_v are rather small with a maximum of 1.8%. The X_v value increases when the curing temperature decreases. It can be related to an increase of the coating free volume, which the water can saturate. For the intermediate temperatures, the X_v are very similar.
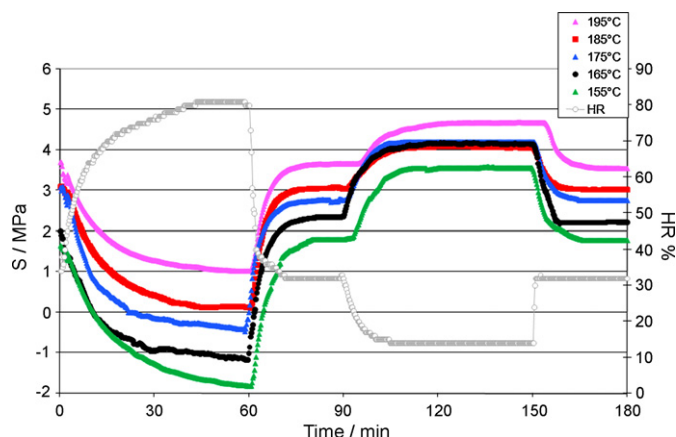

Fig. 1. Water uptake of electrocoatings on phosphatised steel samples according to immersion times in 0.5 M NaCl solution for different curing temperatures.

Fig. 2. Influence of humidity on stress at 25 °C for the coated carbon steel cured at different temperatures.

3.3. Influence of humidity on stress measurements

The calibrated painted samples were placed in the stressmeter at 25 °C and a humidity cycle including four steps was performed. The humidity varied (1) from 35 to 80% RH for 1 h, (2) from 80 to 35% RH for 30 min, (3) from 35 to 15% RH for 1 h and (4) finally from 15 to 35% RH for 30 min.

The influence of humidity on stress at 25 °C shows a clear difference between the systems cured at different temperatures (Fig. 2).

During the high humidity period, water adsorption occurs and induces a compressive stress. On the contrary, during the low humidity period, water desorption generates a tensile stress in the coating as discussed in [12]. The behaviour of both coatings is reversible. Indeed the final stress measured at the end of the cycle is the same as at the beginning under the same conditions of temperature and humidity. This shows that no stress relaxation at all takes place during humidity cycling.

At the beginning of experimentation at 35% RH the measured stress corresponds to residual stress which is built at the interface during the coating curing. Under ambient conditions stress is higher in the paint cured at higher temperatures, showing thereby a higher crosslinking density (Fig. 2). Stress is concentrated near the metal–polymer interface and can therefore alter the interface stability. Moreover, increased built-in stress is related to a better adhesion at the metal–polymer interface [5]. This prevents stress relaxation as well as the motion of the coating segments.

The initial stress is tensile and humid air reduces it (Fig. 2). The stress gaps obtained between 35 and 80% RH and 35 and 15% increase when the curing temperature decreases. The coating which has a high crosslinking after curing at 195 °C, is less sensitive to hygroscopic stress. This effect correlates with data given in Fig. 1, showing a decrease in water uptake for high crosslinked polymers.

3.4. Influence of filiform corrosion initiation by HCl on non-scratched painted aluminum alloy samples

The coated Al6016 samples were placed under the same operating conditions as the normalized test in filiform corrosion in order to test the influence of HCl on the performances of intact coatings (Table 3). Four series of Al samples were analysed by EIS according to the following procedure:

- After painting, samples A were analysed by EIS. The coating capacitance, measured after 10 min in NaCl 0.5 M immersion, was considered as the coating capacitance of the dry film. The samples of series B and C were placed in HCl vapours for 1 h, in order
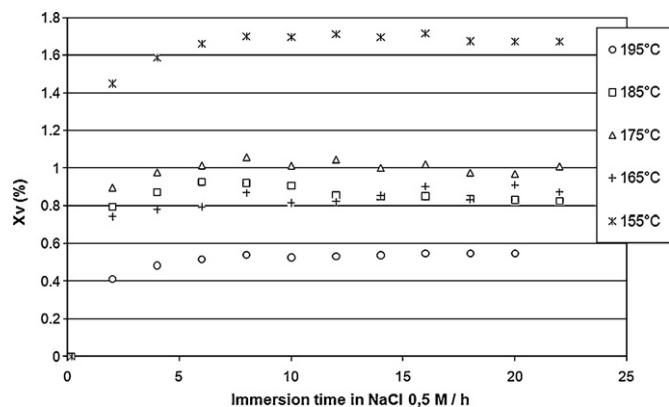
Table 3
Modulus (Z) at 0.01 Hz (Ω) and water uptake (X_v in %) of Al6016 samples according to time for different curing temperatures: (A) after painting, (B) after 1 h in HCl, (C) after 1 h in HCl and 21 days in climatic chamber (40 °C and 82% RH), (D) after 21 days at room temperature (23 °C and 40% RH).

Curing temperature (X)	Series A		Series B		Series C		Series D	
	Z	X_v	Z	X_v	Z	X_v	Z	X_v
195	3.3E09	0.5	4.8E06	3.0	4.8E06	4.7	3.2E09	1.3
185	2.4E09	0.8	2.0E06	3.0	3.0E06	5.1	2.0E09	0.8
175	1.2E09	0.9	5.1E06	2.6	5.7E06	6.1	6.2E08	0.9
165	6.3E09	0.9	1.4E06	2.9	l.3E06	7.4	1.7E08	1.2
155	1.0E09	1.6	2.0E06	3.9	3.0E06	6.8	1.6E09	1.8

to simulate the conditions used to initiate filiform corrosion. EIS measurements were carried out on samples of series B after this first step. The samples of series C were placed for 21 days in a climatic chamber (40 °C and 82% RH) before measuring, in order to simulate the conditions under which filiform corrosion takes place.

- Samples D were placed for 21 days at room temperature (25 °C and 40% RH).

Table 3 shows the impedance modulus at 10 mHz according to time at different curing temperatures. The value of the modulus gives away information about the properties of the film such as wet adhesion and porosity.

For series A and D, the impedance modulus values are between 10^8 and 10^{10} Ω. The stability of the coatings is almost maintained for 21 days under ambient conditions. However, as shown in Table 3, after 21 days of exposure at ambient conditions, the low frequency impedance modulus seems to increase altogether with an increase of curing temperature.

The coating porosity (water uptake) increases and the adhesion stability of the interface may decrease with curing temperature, due to lower crosslinking density and lower density of coating–metal bonds.

For series B and C, the low frequency impedance modulus at 10 mHz are lower than 10^7 Ω (Table 3); the coatings significantly loose their protection properties due to exposure to HCl vapours. It means that, in a classical filiform test, the exposure to HCl vapours not only initiates filiform corrosion in the defect of the coating, but also reduces the stability of the metal polymer interface. In the vapour phase HCl is not a charged species, and the diffusion of the molecule to the interface can quickly appear. HCl can chemically interact with aluminum, which consequently leads to loose of adhesion and decrease of the interfacial impedance. However, further exposure of the samples contaminated by HCl in the climatic chamber for filament growing (samples C, Table 3) does not decrease the modulus more.

The coatings water uptake (Table 3) were determined from capacitance data obtained at high frequencies. For samples of series D, water uptake is very similar to that of series A. For samples of series B submitted to HCl vapours, water uptake is ranging between 2.5 and 4%. For samples of series C, X_v is higher than for series B samples and this effect seems to be increasing with the decrease of the curing temperature. These results confirm that HCl induces hydrophilic locations in the coating or at the metal–coating interface.

3.5. SKP

3.5.1. Initiation of filiform corrosion

Previous research on filiform corrosion had already investigated the process of filaments propagation but the initiation had seldom been studied. In order to understand the role of the coating in filiform corrosion, the corrosion of a non-coated aluminum sample with local HCl deposition was studied. Al6016 panel was masked by

a tape leaving a line with bare metal of 1 mm wide. After exposure to HCl vapours the tape was removed, the metal around contamination was gently degreased with ethanol and was SKP scanned. The corrosion products formed in the line during HCl deposition locally increased the metal potential by 0.4 V (Fig. 3a). This correlates with previous observation concerning the influence of corrosion products on the aluminum potential [23–25]. The topography shows that the corrosion products distribution inside the line was not uniform and that their height varied from 10 to 60 μm. The sample was exposed for 12 h in a climatic chamber under the conditions used for filaments growth (40 °C, 80% RH). From the line of contaminated Al the new corrosion spreading was observed (Fig. 3a). A new-formed thin layer of corrosion products thereby increased the potential around the defect (Fig. 3b). Additionally the contour
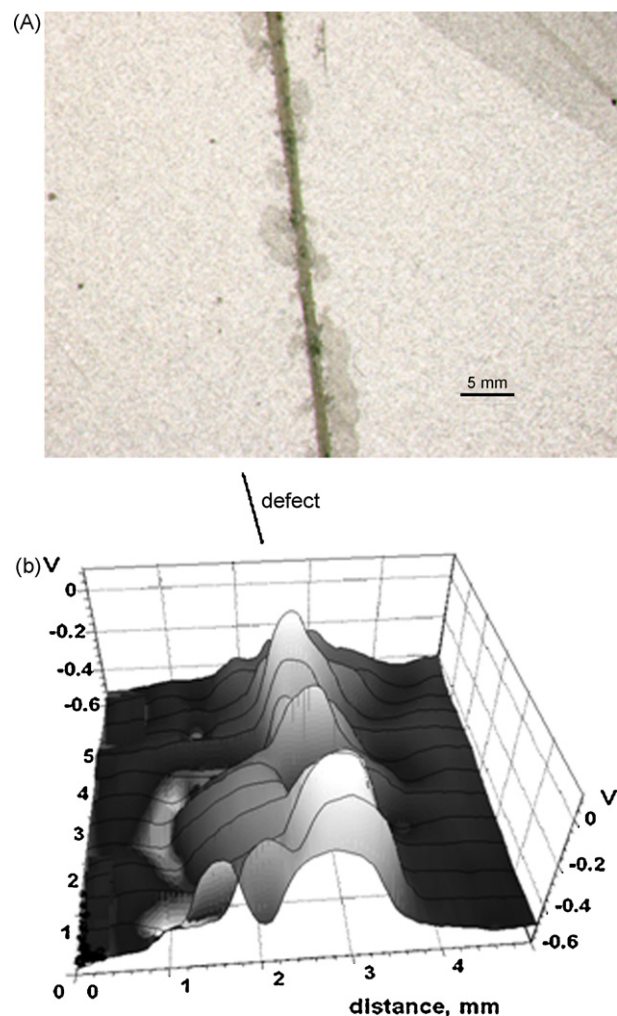

Fig. 3. Photo picture (a), potential profiles (b) for Al6016 surface locally polluted by HCl. Sample was exposed for 12 h in climatic chamber.

with low potential (−0.6 V) around corroding locations could be observed on the SKP map measured in humid air (Fig. 3b). Additional exposure in climatic chamber for 24 h led to a thickening of the corrosion products layer that increased the potential in corroding locations by 0.1 V and spread around the original line over a width of 4–5 mm. From these data we can say that the spreading of corrosion from the locally contaminated aluminum surface takes place without deposition of any polymeric coating. Due to the non-uniformity of the potential the galvanic cell which drives the spreading can be described. Al areas with corrosion products with more positive potential can be more cathodic and the bare aluminum nearby the corroding locations can be more anodic.

Fig. 4 shows the potential maps measured after 3 exposure days of sample cured at 155 °C. Measurements are performed for the same area in the air and in nitrogen at 95% RH. In the air, in the center of the scratch, the potential map shows areas with more positive corrosion potentials and with low potential anodic locations which concentrate at the boundary between the defect and coating. By replacing the air by nitrogen during 2 h, the potential inside and around the defect decreases, showing thereby where cathodic reactions take place. The potential in the defect varies by 0.35 V, which proves that the cathodic reaction is mainly related to the defect. Around the defect the potential also decreased due to underfilm metal corrosion.

Fig. 5 shows the SKP results obtained for the paint cured at 165 °C. After 1 day of exposure, blistering at the boundary between the defect and paint appears in the topography map (Fig. 5a and b). Below blisters the interface shows low potentials (−0.55 V), which indicates that blisters are local anodes. The metal surface in the defect shows noble potentials where oxygen reduction is taking place. After 3 days of exposure (Fig. 5c and d) the scanning was repeated. Air–nitrogen transitions at 95% RH decreased the potential inside the defect, showing thereby that the scratch (1 mm width) is a cathode. Local anodes with low potential were observed
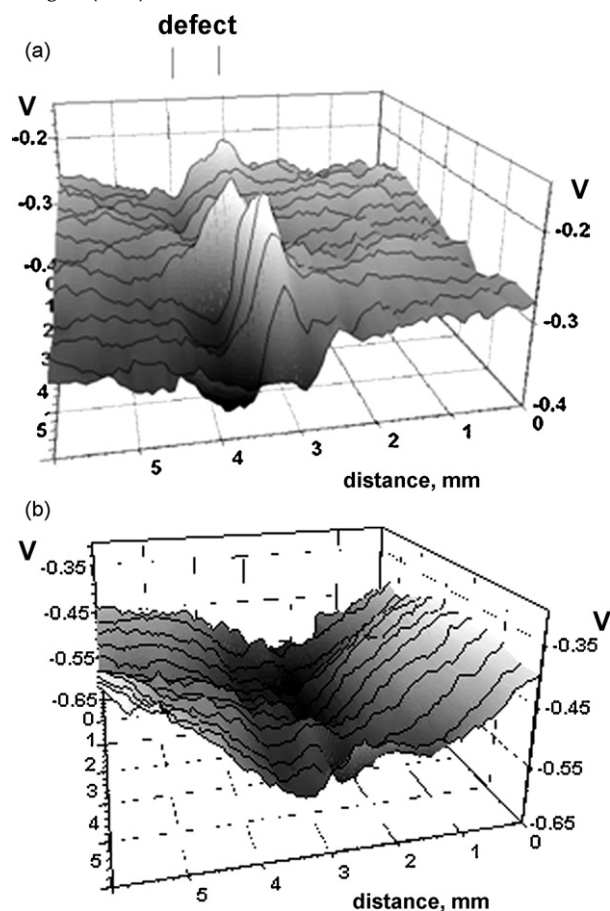

Fig. 4. Potential profiles measured in the air (a) and in nitrogen (b) at 95% RH. Sample was exposed for 3 days and paint was cured at 155 °C.
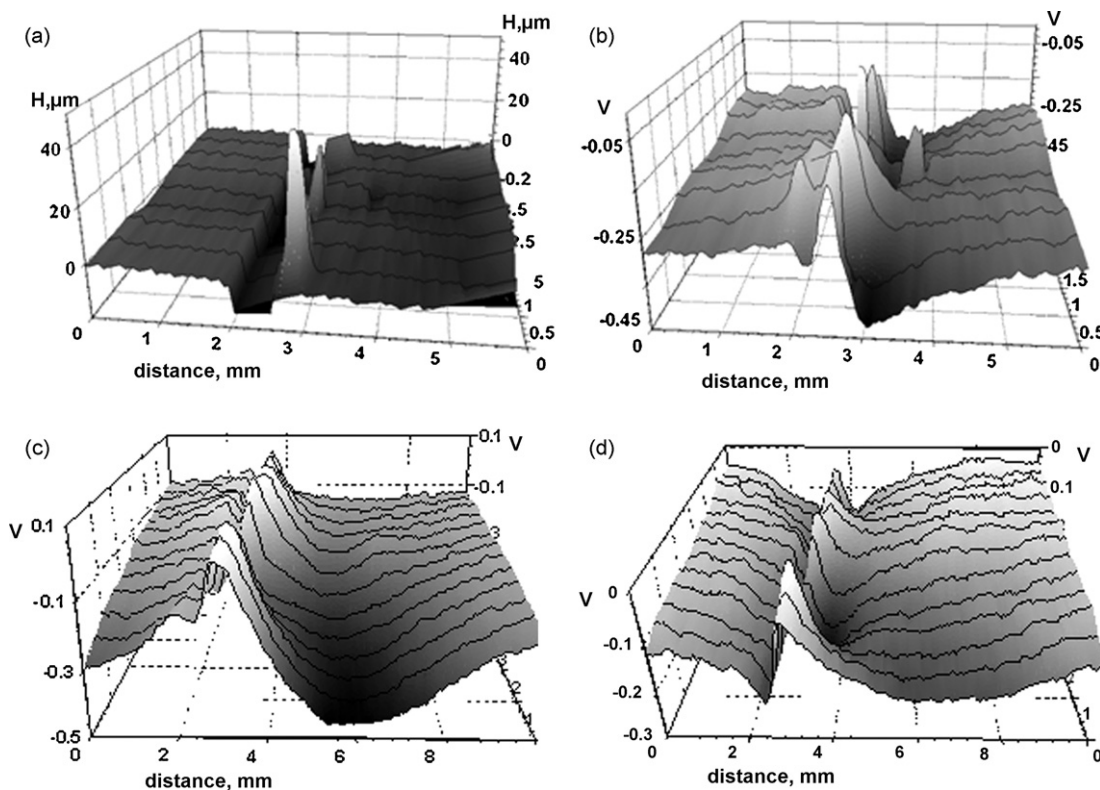

Fig. 5. Paint was cured at 165 °C. Topography (a) and potential profiles (b–d). The sample was exposed during 1 day (a and b) and 3 days (c and d). Measurements were performed in humid air (a–c) and humid nitrogen (d).
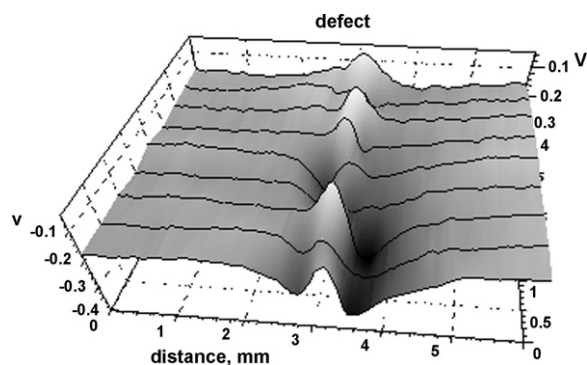
Fig. 6. Curing temperature of 195 °C. Measurements were performed, after 1 day of exposure, in the air at 95% RH.

at the boundary defect–intact paint. The map (Fig. 5c) shows that after 3 days of exposure the local anode spreads underneath the coating at 2 mm from the defect.

Fig. 6 shows the initiation of filiform corrosion of the paint cured at 195 °C. After 1 day of exposure the anodic and cathodic locations were developing inside the defect. Therefore cathodic and anodic places were located in the defect. The exposure went on for 3 days (Fig. 6). No significant spreading under the coating was observed at that time for the scanned area. One can conclude that the center of the scratch is mainly cathodic and that the boundary defect–intact paint develops the local anodes.

To sum it up, the initiation of filiform corrosion from the defect leads to the formation of a galvanic couple. The center of the defect mainly works as a cathode for oxygen reduction and the boundary defect–intact coating creates local anodes. In general this mechanism is almost the same for all coatings. However, after 3 days of exposure, the spreading of corrosion beneath the coatings proved to be different. Therefore, we can assume that relatively uniform undermining takes place for the coating cured at 155 °C. Local anodes appear at the boundary defect–adherent paint cured at 165 °C, which seems to cause spreading of the filaments from the defect. The same geometry of the galvanic cell was observed for the paint cured at 195 °C, but no sufficient spreading of the anodes from the defect took place during the initiation period.

3.5.2. Investigation of the filament propagation

The potential was measured during air–nitrogen–air atmosphere cycling at 95% RH for the sample cured at 175 °C, in order to test the decrease of oxygen concentration to at different locations of the corroding surface. In humid air and in the presence of corrosion activating species, the measured potential corresponds to corrosion potential. It depends on the efficiency of the cathodic reaction and by removing the oxygen this potential shifts to more negative values. The probe was located above the surface and the potential was monitored in humid air until steady state conditions were reached. The air was then replaced by nitrogen at the same humidity (Fig. 7). At the beginning of the filiform corrosion test (3 days) the largest variations (650 mV) of the potential were observed inside the scratch (Fig. 7a). The potential varied by 150 mV at a distance of 1 mm from the defect and only by 30 mV above the intact metal–paint interface measured at a distance of 20 mm from the defect (Fig. 7a).

Similar measurements were repeated after 21 days of exposure. The measurement was performed inside the defect, close to the filament and outside the filament. According to the atmosphere used, air or nitrogen, the potential varied from 250 to 50 mV respectively (Fig. 7b). This indicates that at the beginning, the cathodic reaction is very effective in the defect and supplies the current to the surrounding anodic locations. During exposure the efficiency of the
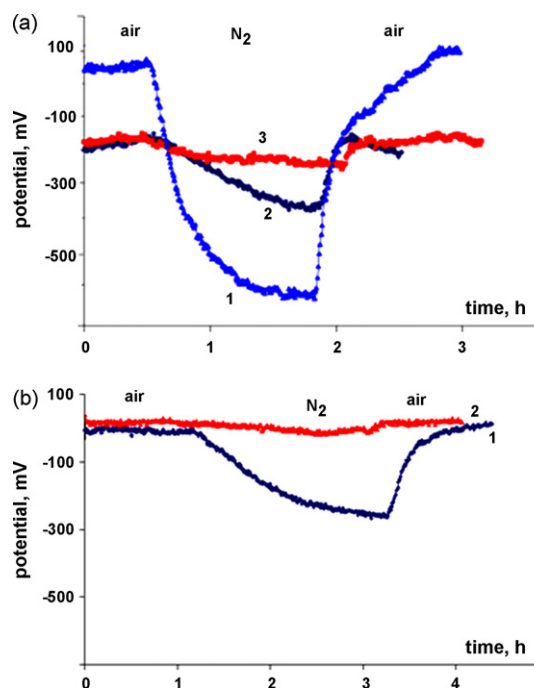

Fig. 7. Variation of the potential (paint curried at 175 °C) during air–nitrogen–air cycling at 95% RH. (a) After 3 days of exposure and (b) after 21 days of exposure. Measurements were done inside the scratch: 1a, 1b, 2b; and above the paint: 1 mm from the scratch (2a) and 20 mm (3a).

reaction in the defect decreased due to the formation of corrosion products but close to the filament, the cathode was efficient enough to maintain the anodic reaction in the filament.

The propagation of filaments after exposure in climatic chamber during 21 days was studied for sample cured at 155 °C. Topography and potential profile are shown in Fig. 8. The area with decreased potentials is related to the intact paint. The potentials are increased in and around the defect. Some blisters were found close to the defect but they did not show the potentials of active dissolution (Fig. 8). The paint around the defect had low adhesion and could be easily delaminated. We can assume that the corrosion uniformly spreads from the defect underneath the coating without spatial separation of anodic and cathodic locations (Fig. 8). The air–nitrogen potential transitions were 100 mV. The width of this area was 2–2.5 mm. This correlates with disbonding phenomena observed in [10].

The sample, cured at 165 °C and exposed in the climatic chamber for 21 days, shows filiform corrosion. The topography and potential profiles for the filament spreading from the defect are given in Fig. 9. In humid air the head of the filament has potential of 300 mV more negative than the intact metal paint interface. It corresponds to the active anode containing hydrolyzed species of $AlCl_3$ [7]. The tail shows more positive potentials due to the formation of corrosion products $Al(OH)_3$ and $Al(OH)(CO_3)$ [7]. By replacing humid air by nitrogen, the potential of the head, the tail and the surface in the scratch decreases by approximately 100–150 mV (Fig. 9b and c). As a result, the cathodic process is distributed over the surface of the corroding location.

Filaments can be seen on samples cured at 185 °C (Fig. 9d). The filaments are small (about 2 mm). They are located close to the defect and almost without any "tail". The boundary defect–intact paint shows low anodic potentials and the defect is noble. Replacing humid air by nitrogen during 2 h reduces the potential in the defect by 170–200 mV and in active locations in filaments by 150–180 mV. It shows that oxygen reduction during the propagation of the filament takes place in the defect and above the active filament.
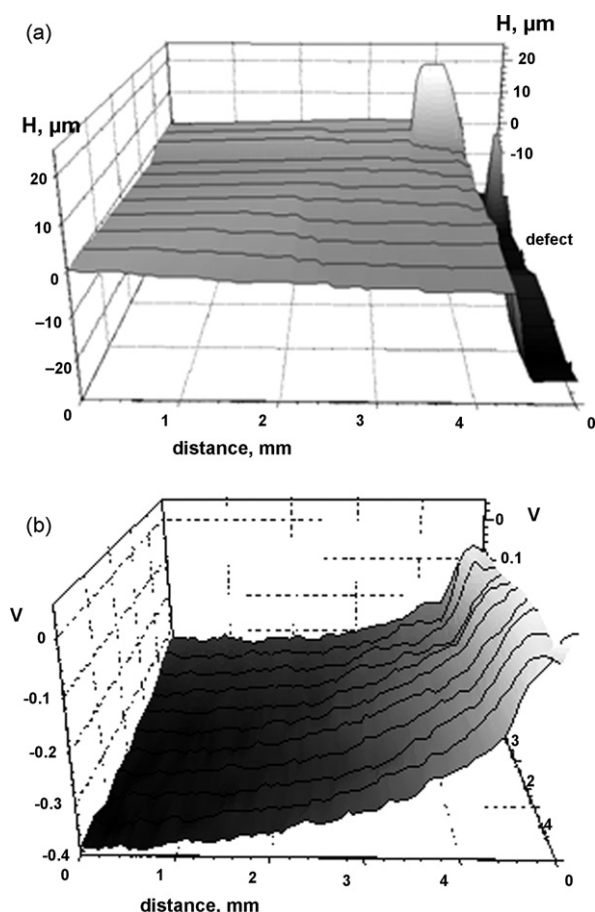
Fig. 8. Topography (a) and potentials (b) in the air at 95% RH for sample cured at 155 °C and exposed for 21 days.

Additionally the parts of the interfaces without filaments were also scanned. An increase of the potentials around the defect was observed (e.g. see Figs. 8b and 9b). This is generally related to a thickening of the surface oxide and can be observed thanks to the deposition of corrosion products [23–25]. The width of these areas developed from the scratch after 21 days of exposure was correlated with the curing temperature (Fig. 10). The highest creep was observed for curing at low temperature and uniform corrosion could not spread under the joint after curing at high temperature.

The potential of the intact metal–paint interface was measured outside the defect after a 21 days test in the chamber. The paint cured at 155 °C has a potential close to the bare aluminum. It may be due to minor interface interaction. By raising the curing temperature, the potential above intact polymer coating goes up and this can be related to an increase of adhesion at the aluminum–paint interface in wet air conditions (Fig. 10). One may assume that improved interface inhibits uniform spreading and concentrates the corrosion to local corrosion events (filaments). These results correspond to those observed in the classical filiform corrosion test examined in a previous paper [10]. Indeed, after 21 days of exposure, a decrease of curing temperature induces a delamination phenomenon instead of filiform corrosion.

4. Discussion

In the first part of the study, it was shown that, by increasing the curing temperature, the polymer crosslinking and the residual stress which is developed at the interface also increased. On the other hand, it results in a decrease of water uptake. The mechan-

ical properties of organic coatings and coating–substrate interface have significantly shown the influence on initiation and propagation of filiform corrosion. The deformability and strong adhesion of the coating are influenced by the resistance to filiform corrosion [28–30]. Stronger adhesion increased the anodic attack depth of the metal at the interface [28]. Increasing the crosslinking can increase the amount of groups anchoring to the metal oxide. Increased curing temperature can provide the interfacial layer with improved interaction. The high crosslinked polymer shows a more intact and stable-to-hydrolyze interface. As a result, the samples in the water electrolyte show a high impedance modulus at low frequency range (Table 3). Moreover, increased polymer crosslinking produces a residual stress (Fig. 2) which, on its turn, can raise the coating ability to peel out from the substrate. It was shown [31] that for painted carbon steel the maximum impedance modulus is obtained when the paint is cured in a range of temperatures between 155 and 185 °C. The impedance decreases significantly when the paint is cured at lower and higher temperatures. This may prove the double effect of crosslinking on joint stability.

The aluminum samples cured at low temperature show a quick delamination around the defect without formation of filaments (Figs. 4 and 8). A similar spreading of the corrosion from the corroding location takes place on the surface of bare aluminum. Increasing the paint adhesion leads to filiform corrosion where the interface locally allows low potential of active metal dissolution. A further increase of adhesion makes the anodic front propagation more difficult. For the coatings cured at high temperatures the anodic reaction is located near the defect (Fig. 9d). The ability to propagation was mainly observed for the coating cured at 165 °C (Fig. 9a and b). The paints with increased curing temperature show narrower filaments that can be a result of increased adhesion to substrate [10].

Scientific research has shown that filiform corrosion of aluminum alloys is a result of the formation of a galvanic cell and anodic undermining of the paint [5–9]. It fully corresponds to these SKP data for cataphoretic coatings on AA6016 alloy. The initiation of aluminum corrosion in the defect produces a galvanic couple where the defect is the cathode and the metal underneath the intact paint around the defect is the anode. The spatial separation of the electrochemical reactions and the galvanic couple efficiency are determined by the rates of cathodic and anodic reactions. The highest current of this cell corresponds to an effective oxygen reduction on the surface of corroding aluminum and to an easy migration of the chloride ions to the interface where aluminum anodic dissolution takes place. It was shown that, at the beginning of corrosion, the cathodic reaction in the defect is very effective. The cathodic current which is picked in the defect will be directed to the anodic locations of the growing filaments. The low potential (anodic) areas are going further than the visible area of paint lifting (blister, Fig. 5a and c). It may be due to chloride ions which migrate out from the defect along the metal–paint interface and which activate the metal anodic dissolution and further filament growth. The geometry and amount of active anodic places are dependent on the ionic conductivity and on the stability of the surrounding metal–polymer interface. Later on, however, the cathodic efficiency may decrease due to the formation of corrosion products in the defect. When the filament's head moves away from the defect, its influence on filament propagation will decrease. In this case the filament tail will be cathode in the galvanic cell (Fig. 9b and c). The topography of the filament corresponds to the potentials profile (Fig. 9a and b).

In general, the galvanic cell formation takes place when in contact with two dissimilar metals. The electromotive force of this cell is determined by the difference in potentials. Additionally, the difference in potentials for the same metal surface may appear in the concentration element. However, at the beginning, it is difficult to induce the differential aeration cell inside the defect and intact metal–paint interface. One may assume that the spatial separation
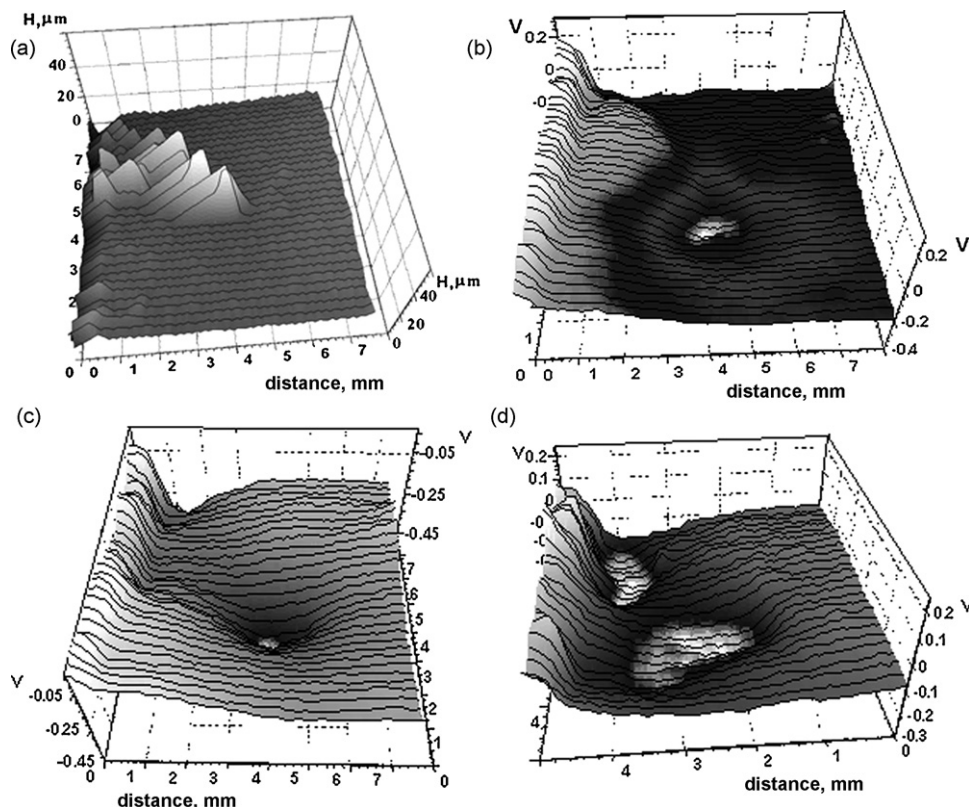
Fig. 9. Topography (a) and potential profiles (b–d) after 21 days of exposure. (b and c) The filament under the paint cured at 165 °C and (d) at 185 °C. Measurements were performed at 95% RH in the air (a, b, and d) and in nitrogen (c).

of two electrochemical reactions can be due to the difference in efficiencies (Tafel slopes) of cathodic and anodic reactions. The corrosion process inside the confined defect may have anodic control. This is confirmed by the fact that chloride deposition and aluminum corrosion raises the defect potential. In order to remove the control, the corroding system increases the anodic process efficiency and the chloride ions migrate to metal–paint interface and provoke a coating anodic undermining [25]. During filament propagation the potential gradient is developed. Due to the corrosion products formed in the defect and inside the filament tail, the Al potential increases. In the galvanic couple locations with more positive potential are working as a cathode and low potential aluminum–paint interface nearby will be sensitive to anodic dissolution. We may assume that the difference in the surface potentials may be the driving force of this galvanic cell.
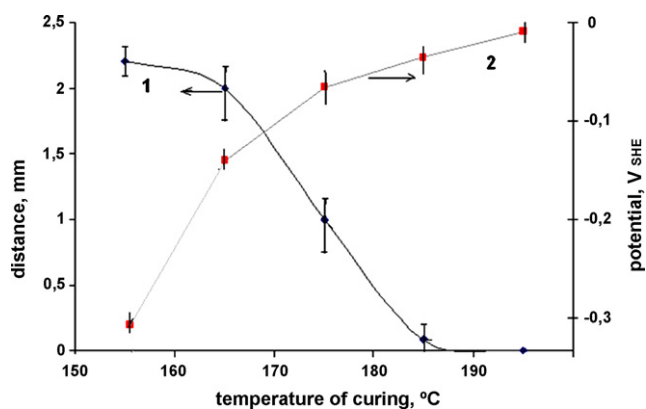
5. Conclusions

A cataphoretic coating was applied at different curing temperatures (from 155 to 195 °C) which lead to a different crosslinking density and different T_g values. The increase of T_g and crosslinking density leads to a film showing a higher value of stress in the same conditions of humidity and temperature. The residual stress is applied to the metal–paint interface which can change its properties. A good correlation is observed between the water uptake and the stress measurement during a humidity cycle: when the curing temperature decreases, the coating is more sensitive to humidity and induces a slight increase in water uptake. The protection properties offered by electrocoatings are very good whatever the curing temperatures in case of substrate pre-treatment.

This study shows the important impact of HCl vapours, which can cause a significant degradation of the system.

SKP measurements revealed that filiform corrosion of the painted aluminum starts from the formation of a galvanic couple: cathode (defect)–anode (boundary of the defect–intact paint). This couple is the same whatever the curing conditions. The cathodic current maintained in the defect can be significant for anodic polarization and propagation of the filament. Increased adhesion between paint and aluminum localizes the uniform spreading to narrow filaments.

Fig. 10. Area width of increased potentials around the scratch (1), potential value on intact metal–polymer interface (2) vs. curing temperature, after 21 days of exposure.

References

[1] A. Bautista, Progress in Organic Coatings 28 (1996) 49.

[2] O. Lunder, B. Olsen, K. Nicancioglu, International Journal of Adhesion & Adhesives 22 (2002) 143.
[3] R.T. Ruggeri, T.R. Beck, Corrosion (Houston) 39 (1983) 452.
[4] H. Leidheiser, W. Funke, JOCCA 70 (1987) 121–132.
[5] H. Kaeshe, Werkstoffe und Korrosion 11 (1959) 668.
[6] G. Grundmeier, W. Schmidt, M. Stratmann, Electrochimica Acta 45 (2000) 2515.
[7] N. Le Bozec, D. Persson, A. Nazarov, D. Thierry, Journal of the Electrochemical Society 149 (2002) B403.
[8] P.P. Leblanc, G.S. Frankel, Journal of the Electrochemical Society 151 (2004) B105–B113.
[9] H.N. McMurray, A.J. Coleman, G. Williams, A. Afseth, G.M. Scamans, Journal of the Electrochemical Society 154 (2007) C339–C348.
[10] A.-P. Romano, M.-G. Olivier, C. Vandermiers, M. Poelman, Progress in Organic Coatings 57 (2006) 400.
[11] D.Y. Perera, P. Schutyser, 22nd FATIPEC Congress, Budapest, Hungary, 1994, p. 1.
[12] D.Y. Perera, Progress in Organic Coatings 28 (1996) 21.
[13] D.Y. Perera, Progress in Organic Coatings 44 (2002) 55.
[14] D.Y. Perera, Progress in Organic Coatings 50 (2004) 247.
[15] R.F. Hamade, D.A. Dillard, International Journal of Adhesion & Adhesives 25 (2005) 147.
[16] G. Bierwagen, Progress in Organic Coatings 28 (1996) 43.
[17] M. Destreri, J. Vogelsang, L. Fedrizzi, F. Deflorian, Progress in Organic Coatings 37 (1999) 69.
[18] D.M. Brasher, A.H. Kingsbury, Journal of Applied Chemistry 4 (1954) 62.
[19] J. Hölzl, F.K. Schulte, Solid Surface Physics, Springer-Verlag, Berlin/Heidelberg/New York, 1979, p. 2.
[20] S. Trassati, R. Parsons, Pure and Applied Chemistry 58 (3) (1986) 437.
[21] M. Stratmann, H. Streckel, Corrosion Science 30 (1990) 681.
[22] R. Memming, Semiconductor Electrochemistry, Willey, VCH Verlag GmbH, 2001, p. 26.
[23] T.N. Muster, A.E. Hughes, Journal of the Electrochemical Society 153 (2006) B474–B485.
[24] E. Juzeliunas, k. Leinartas, W. Furbeth, K. Juttner, Corrosion Science 45 (2003) 1939.
[25] A. Nazarov, D. Thierry, Electrochimica Acta 49/17–18 (2004) 2717.
[26] A. Nazarov, D. Thierry, Electrochimica Acta 49/17–18 (2004) 2955.
[27] M.-G. Olivier, A.-P. Romano, C. Vandermiers, X. Mathieu, M. Poelman, Progress in Organic Coatings 63 (2008) 323.
[28] H. Leth-Olsen, K. Nisancioglu, Corrosion (Houston) 53 (1997) 705.
[29] G. Williams, H.N. McMurray, Journal of the Electrochemical Society 150 (2003) B380–B388.
[30] J.L. Delplanke, S. Berger, X. Lefebvre, D. Maetens, A. Pourbaix, N. Neymans, Progress in Organic Coatings 43 (2001) 64.
[31] S.J. Garcia, J. Suay, Progress in Organic Coatings 59 (2007) 251.